Inorganic Chemistry

ARTICLE

pubs.acs.org/IC

Syntheses, Crystal and Electronic Structures, and Characterizations of Quaternary Antiferromagnetic Sulfides: Ba_2MFeS_5 (M = Sb, Bi)

Lei Geng,[†,‡] Wen-Dan Cheng,[*,†] Hao Zhang,[†] Chen-Sheng Lin,[†] Wei-Long Zhang,[†] Ye-Yu Li,[†,‡] and Zhang-Zhen He[†]

[†]State Key Laboratory of Structural Chemistry, Fujian Institute of Research on the Structure of Matter, Chinese Academy of Sciences, Fuzhou 350002, People's Republic of China

[‡]Graduate School of the Chinese Academy of Sciences, Beijing 100039, People's Republic of China

Supporting Information

ABSTRACT:

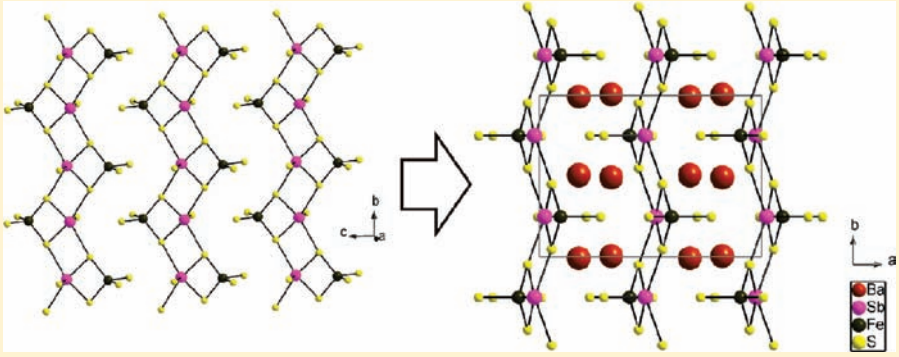

Two new quaternary sulfides, Ba_2SbFeS_5 and Ba_2BiFeS_5, were synthesized by using a conventional high-temperature solid-state reaction method in closed silica tubes at 1123 K. The two compounds both crystallize in the orthorhombic space group *Pnma* with $a = 12.128(6)$ Å, $b = 8.852(4)$ Å, $c = 8.917(4)$ Å, and $Z = 4$ for Ba_2SbFeS_5 and $a = 12.121(5)$ Å, $b = 8.913(4)$ Å, $c = 8.837(4)$ Å, and $Z = 4$ for Ba_2BiFeS_5. The crystal structure unit can be viewed as an infinite one-dimensional edge-shared MS_5 (M = Sb, Bi) tetragonal-pyramid chain with FeS_4 tetrahedra alternately arranged on two sides of the MS_5 polyhedral chain via edge-sharing (so the chain can also be written as $_1^{\infty}[MFeS_5]^{4-}$). Interestingly, the compounds have the structural type of a Ba_3FeS_5 high-pressure phase considering one Ba^{2+} is replaced by one Sb^{3+}/Bi^{3+}, with Fe^{4+} reduced to Fe^{3+} for in order to maintain the electroneutrality of the system. As a result, the isolated iron ions in Ba_3FeS_5 are bridged by intermediate MS polyhedra in Ba_2MFeS_5 (M = Sb, Bi) compounds and form the $_1^{\infty}[MFeS_5]^{4-}$ chain structure. This atom substitution of Ba^{2+} by one Sb^{3+}/Bi^{3+} leads to a magnetic transition from paramagnetic Ba_3FeS_5 to antiferromagnetic Ba_2MFeS_5, resulting from an electron-exchange interaction of the iron ions between inter- or intrachains. Magnetic property measurements indicate that the two compounds are both antiferromagnetic materials with Néel temperatures of 13 and 35 K for Ba_2SbFeS_5 and Ba_2BiFeS_5, respectively. First-principles electronic structure calculations based on density functional theory show that the two compounds are both indirect-band semiconductors with band gaps of 0.93 and 1.22 eV for Ba_2SbFeS_5 and Ba_2BiFeS_5, respectively.

INTRODUCTION

Ternary Ba−Fe−S systems have been well studied, and many compounds have been synthesized and structurally characterized over the past 40 years. Examples include $Ba_7Fe_6S_{14}$,[1] $BaFe_2S_3$,[2] $Ba_6Fe_8S_{15}$,[2] $Ba_{15}Fe_7S_{25}$,[3] Ba_3FeS_5,[3] $Ba_4Fe_2S_{7.3333}$,[4] $Ba_9Fe_4S_{15}$,[5] $Ba_9Fe_4S_{16.72}$,[5] $Ba_9Fe_3S_{15}$,[6] $BaFe_2S_4$,[7] $Ba_2Fe_4S_5$,[8] etc. In these compounds, FeS_4 tetrahedra commonly serve as basic building units under normal conditions, which can further form dinuclear, trinuclear, or tetranuclear complex units in a corner- or edge-sharing manner. Low-dimensional structures of zero-dimensional (0-D) separated polynuclear Fe−S blocks or one-dimensional (1-D) Fe−S chains are mostly witnessed in these crystals. Quaternary compounds in the Ba−Fe−S systems are few, and not until recently were rare-earth elements introduced into these systems, and therefore several new quaternary sulfides $BaLn_2FeS_5$ (Ln = La, Cc. Pr, Nd, Sm) were synthesized and characterized.[9]

On the other hand, ternary Ba−M−S (M = Sb, Bi) compounds are less explored, and only $Ba_8Sb_6S_{17}$,[10] $BaSb_2S_4$,[11] $BaBi_2S_4$,[12] and $Ba_3Sb_{4.66}S_{10}$,[13] are reported to date. Quaternary compounds in these systems are even fewer, and only $BaLaBi_2S_6$[14] and $Ba_{2.62}Pb_{1.38}Sb_4S_{10}$[13] can be found in the ICSD

Received: October 28, 2010
Published: February 18, 2011

database (Inorganic Crystal Structure Database, Fachinformationszentrum Karlsruhe, Karlsruhe, Germany, and U.S. Department of Commerce, released in 2009). In addition, many antimony and bismuth chalcogenides manifest astonishingly rich structures and diverse properties, which are commonly believed from their asymmetric coordination environments to be induced by the stereochemically active ns^2 lone-pair electrons on the Sb^{3+} and Bi^{3+} ions.[15] Therefore, we attempted to introduce element Sb or Bi into the quaternary Ba−M−Fe−S (M = Sb, Bi) systems, and extensive explorations resulted in the discovery of two new compounds Ba_2MFeS_5 (M = Sb, Bi).

The two title compounds are isostructural, and both crystallize in the structural type of a Ba_3FeS_5 high-pressure phase, in which one Ba^{2+} ion is substituted by a Sb^{3+}/Bi^{3+} and the valence state of the iron ion is reduced from Fe^{4+} to Fe^{3+} in order to maintain the electrical neutrality.[3] As a result, the isolated iron ions in Ba_3FeS_5 are bridged by intermediary Sb/Bi−S polyhedra in Ba_2MFeS_5 and form the $_1^{\infty}[MFeS_5]^{4-}$ chain structure. The chain is composed of an infinite 1-D edge-shared MS_5 tetragonal-pyramid chain with FeS_4 tetrahedra alternately connected on both sides of the MS_5 polyhedral chain via edge sharing. Magnetic property measurements indicate that both compounds are antiferromagnetic with Néel temperatures of 13 and 35 K for Ba_2SbFeS_5 and Ba_2BiFeS_5, respectively. We expect that electron-exchange interactions of iron ions might occur between an inter- or intrachain of $_1^{\infty}[MFeS_5]^{4-}$ in the compounds because of the short Fe−Fe distances of ∼5.842 Å in Ba_2SbFeS_5 and ∼5.865 Å in Ba_2BiFeS_5 by comparison with that of Ba_3FeS_5. First-principles electronic structure calculations based on density functional theory (DFT) show that the two compounds are both indirect-band semiconductors with band gaps of 0.93 and 1.22 eV for Ba_2SbFeS_5 and Ba_2BiFeS_5, respectively. In this work, we present the syntheses, crystal and electronic structures, and optical and magnetic characterizations of the two compounds.

EXPERIMENTAL SECTION

Syntheses. Single crystals of Ba_2MFeS_5 (M = Sb, Bi) were synthesized by a conventional high-temperature solid-state reaction method in evacuated silica tubes at 1123 K. Starting materials of BaS (99.7%, Alfa), Fe (99.98%, Alfa), Sb (5N, Sinopharm Chemical Reagent Co., SCRC), Bi (5N, SCRC), and S (99.5%, SCRC) were used without further treatment. According to the molar ratio of 2:1:1:5 Ba/Sb(Bi)/Fe/S, 2.6 mmol of BaS, 1.3 mmol of Sb (or Bi), 1.3 mmol of Fe, and 3.9 mmol of S were mixed roughly, transferred into predried graphite crucibles, and subsequently flame-sealed in evacuated silica tubes under 10^{-2} Pa. The tubes were placed in a resistance furnace and heated to 1123 K in 50 h under operation by a temperature controller. After holding at 1123 K for 30 h, the samples were slowly cooled to 773 K in 200 h, followed by cooling to room temperature in 50 h. Bulk crystals of Ba_2SbFeS_5 and Ba_2BiFeS_5 were obtained, and both of them were black.

X-ray Crystallography. Single crystals of Ba_2MFeS_5 (M = Sb, Bi) were selected and mounted on glassy fibers for X-ray diffraction (XRD) measurements. Data collections were carried out on a Rigaku SCX mini diffractometer equipped with graphite-monochromated Mo Kα radiation (λ = 0.710 73 Å) at 293(2) K. The Rigaku *CrystalClear* (version 1.4) program package was used for diffraction image collection and data reduction. Lorentz and polarization effects and multiscan semiempirical corrections were applied to the intensity data.

The crystal structures were solved by direct methods and refined by full-matrix least squares on F^2 using the *SHELXL-97* program.[16] All of the atom sites in the unit cell are ordered with fully occupied according to site-occupancy refinements. Anisotropic thermal parameter refinements were applied to all of the atoms. The program *PLATON* was used to check the final refined crystal structures of Ba_2MFeS_5 (M = Sb, Bi), and no missed or higher symmetry elements were found. X-ray energy-dispersive spectroscopy (EDS; Oxford INCA) analysis on a field-emission scanning electron microscope (JSM6700F) also confirmed Ba/M/Fe/S molar ratios of 1.18:0.58:0.477:2.32 (for M = Sb) and 1.10:0.59:0.44:2.41 (for M = Bi), which are in reasonable agreement with the stoichiometric proportions from their single-crystal X-ray structural analyses. Detailed crystallographic data and refinement results are summarized in Table 1. The atomic coordinates, equivalent isotropic thermal parameters, and selected bond distances for Ba_2MFeS_5 (M = Sb, Bi) are listed in Tables 2 and 3.

Powder XRD patterns of both compounds were recorded on a Rigaku MiniFlex II diffractometer with Cu Kα radiation. The scanning range is 5−65° in 2θ with a step size of 0.01°. The experimental and simulated

Table 1. Crystal Data and Structural Refinement Details for Compounds Ba_2SbFeS_5 and Ba_2BiFeS_5

chemical formula	Ba_2SbFeS_5	Ba_2BiFeS_5
fw	612.58	699.81
space group	*Pnma*	*Pnma*
a (Å)	12.128(6)	12.121(5)
b (Å)	8.852(4)	8.913(4)
c (Å)	8.917(4)	8.837(4)
V (Å^3), Z	957.3(8), 4	954.8(7), 4
ρ_{cal} (g cm^{-3})	4.250	4.868
abs corrn	multiscan	multiscan
abs coeff (mm^{-1})	13.400	29.012
cryst size (mm)	0.22 × 0.15 × 0.10	0.26 × 0.20 × 0.18
F(000)	1076	1204
R1[a], wR2[b], for $I > 2\sigma(I)$	0.0214, 0.0537	0.0333, 0.0788
R1[a], wR2[b], for all data	0.0233, 0.0673	0.0360, 0.1039
GOF on F^2	1.222	1.159

[a] $R1 = \Sigma||F_o| - |F_c||/\Sigma|F_o|$. [b] $wR2(F_o^2) = [\Sigma w(F_o^2 - F_c^2)^2/\Sigma w(F_o^2)^2]^{1/2}$.

Table 2. Atomic Coordinates and Equivalent Isotropic Displacement Parameters (Å^2) for Compounds Ba_2MFeS_5 (M = Sb, Bi)

atom	Wyckoff	x	y	z	U_{eq}[a]
			Ba_2SbFeS_5		
Ba(1)	8d	0.3229(1)	0.0069(1)	0.3777(1)	0.013(1)
Sb(1)	4c	0.0231(1)	0.2500	0.5181(1)	0.013(1)
Fe(1)	4c	0.0947(1)	0.2500	0.1707(1)	0.012(1)
S(1)	8d	0.0543(1)	0.0486(1)	0.3221(1)	0.014(1)
S(2)	4c	0.2108(2)	0.2500	0.6158(2)	0.014(1)
S(3)	4c	0.2746(2)	0.2500	0.1140(2)	0.014(1)
S(4)	4c	0.4930(1)	0.2500	0.5348(2)	0.015(1)
			Ba_2BiFeS_5		
Ba(1)	8d	0.3226(1)	0.0089(1)	0.3834(1)	0.014(1)
Bi(1)	4c	0.0173(1)	0.2500	0.5327(1)	0.015(1)
Fe(1)	4c	0.0948(1)	0.2500	0.1721(2)	0.012(1)
S(1)	8d	0.0552(2)	0.0457(3)	0.3185(2)	0.016(1)
S(2)	4c	0.2146(3)	0.2500	0.6263(3)	0.014(1)
S(3)	4c	0.2751(2)	0.2500	0.1165(3)	0.015(1)
S(4)	4c	0.4946(3)	0.2500	0.5370(3)	0.014(1)

[a] U_{eq} is defined as one-third of the trace of the orthogonalized U_{ij} tensor.

dx.doi.org/10.1021/ic102597y |*Inorg. Chem.* 2011, 50, 2378–2384

Table 3. Selected Bond Lengths (Å), Bond Valences (BV), and Bond Valence Sums (BVS) of Cations for Compounds Ba_2MFeS_5 (M = Sb, Bi)[a]

	distance	BV		distance	BV
			Ba_2SbFeS_5		
Ba(1)−S(3)	3.2407(16)	0.279	Sb(1)−S(1)#5	2.5249(15)	0.871
Ba(1)−S(4)#1	3.2812(16)	0.251	Sb(1)−S(1)#6	3.1457(16)	0.163
Ba(1)−S(2)#2	3.2856(16)	0.247	Sb(1)−S(1)#7	3.1457(16)	0.163
Ba(1)−S(4)	3.2934(17)	0.242	Sb(1)−S(3)#8	3.2354(23)	0.128
Ba(1)−S(2)	3.3142(16)	0.229		ΣBVS =	3.298
Ba(1)−S(1)	3.316(2)	0.228	Fe(1)−S(4)#9	2.209(2)	0.850
Ba(1)−S(3)#3	3.3184(16)	0.227	Fe(1)−S(3)	2.240(2)	0.782
Ba(1)−S(1)#4	3.3441(17)	0.211	Fe(1)−S(1)#5	2.2896(15)	0.684
	ΣBVS =	1.915	Fe(1)−S(1)	2.2896(15)	0.684
Sb(1)−S(2)	2.438(2)	1.102		ΣBVS =	3.000
Sb(1)−S(1)	2.5249(15)	0.871			
			Ba_2BiFeS_5		
Ba(1)−S(3)	3.242(2)	0.278	Bi(1)−S(1)#5	2.666(2)	0.771
Ba(1)−S(2)#1	3.270(2)	0.258	Bi(1)−S(1)#6	3.074(2)	0.256
Ba(1)−S(4)#2	3.276(3)	0.254	Bi(1)−S(1)#7	3.074(2)	0.256
Ba(1)−S(4)	3.288(3)	0.246	Bi(1)−S(3)#8	3.218(3)	0.174
Ba(1)−S(2)	3.307(2)	0.234		ΣBVS =	3.343
Ba(1)−S(1)	3.308(3)	0.233	Fe(1)−S(4)#9	2.211(3)	0.846
Ba(1)−S(3)#3	3.313(2)	0.230	Fe(1)−S(3)	2.240(4)	0.782
Ba(1)−S(1)#4	3.352(3)	0.207	Fe(1)−S(1)#5	2.285(3)	0.692
	ΣBVS =	1.940	Fe(1)−S(1)	2.285(3)	0.692
Bi(1)−S(2)	2.531(3)	1.114		ΣBVS =	3.013
Bi(1)−S(1)	2.666(2)	0.771			

[a] Symmetry transformations used to generate equivalent atoms: #1, $-x + {}^1/_2, -y, z - {}^1/_2$; #2, $-x+1, -y, -z+1$; #3, $-x + {}^1/_2, -y, z + {}^1/_2$; #4, $x + {}^1/_2, y, -z + {}^1/_2$; #5, $x, -y + {}^1/_2, z$; #6, $-x, y + {}^1/_2, -z+1$; #7, $-x, -y, -z+1$; #8, $x - {}^1/_2, -y + {}^1/_2, -z + {}^1/_2$; #9, $x - {}^1/_2, y, -z + {}^1/_2$.

powder XRD patterns of Ba_2MFeS_5 (M = Sb, Bi) are shown in Figure S1 in the Supporting Information.

UV−Vis−NIR Spectroscopy Measurements. The UV−vis−NIR diffuse-reflectance spectra were recorded on a PerkinElmer Lambda 900 UV−vis−NIR spectrometer in the range of 600−3000 nm at room temperature. A $BaSO_4$ plate was used as the reference material. The optical absorption spectra were converted from diffuse-reflectance spectra using the Kubelka−Munk function, $\alpha/S = (1-R)^2/2R$, where α is the Kubelka−Munk absorption coefficient and R is the scattering coefficient.

Magnetic Susceptibility. Magnetic susceptibility measurements were performed on polycrystalline powder samples of Ba_2MFeS_5 (M = Sb, Bi) at a magnetic field of 5000 Oe on a Quantum Design MPMS-XL SQUID magnetometer. The direct-current (dc) magnetic moment measurements were carried out over a temperature range of 2−300 K. The susceptibility data from Néel temperature T_N up to 300 K were used to fit the Curie−Weiss equation $\chi = C/(T-\theta)$, where C is the Curie constant and θ is the Weiss constant. The effective magnetic moment μ_{eff} was evaluated from the equation $\mu_{eff} = (7.997C)^{1/2}\mu_B$.[17]

Electronic Structure Calculations. Electronic energy band structures were calculated to provide a further understanding and interpretation of the absorption spectra origin for the compounds synthesized. The crystal structure of Ba_2MFeS_5 (M = Sb, Bi) determined from single-crystal XRD was employed without further geometry optimizations for the calculations. The energy and band structure calculations were performed using the first-principles quantum mechanical program *CASTEP* within the DFT formalism.[18] Pseudopotentials were utilized to describe electron-ion interactions, and a plane-wave basis set was used to represent electronic wave functions in the *CASTEP* program. The Perdew−Burke−Ernzerhof (PBE) functional within the generalized gradient approximation scheme was employed to calculate the exchange−correlation parameters.[19] Norm-conserving pseudopotentials were employed for all of the atoms in the reciprocal representation.[20] A 3 × 2 × 4 Monkhorst−Pack k-point mesh was selected in the energy calculations, and a plane-wave cutoff energy of 550 eV was set to determine an optimal level of the total energy convergence for the two compounds. Pseudo atomic calculations were performed for S $3s^23p^4$, Fe $3d^64s^2$, Sb $5s^25p^3$, Bi $5d^{10}6s^26p^3$, and Ba $5s^25p^66s^2$. A 1 × 2 × 1 supercell along the direction of the ${}_1^{\infty}[MFeS_5]^{4-}$ chains was constructed for the electronic structure calculations because the antiferromagnetic interaction of the intrachain is stronger than that of the interchain. The local-density approximation (LDA) + U approach (with Hubbard U = 2.5 eV) is also included for correlation effects in the DFT calculations.[21] The possible spin-polarization configurations of Fe^{3+} ions with lowest energy were considered in the final electronic structure and density of state (DOS) calculations (see Figure S2 in the Supporting Information). The rest of the parameters used in the calculations were set by the default values of the *CASTEP* code.

RESULTS AND DISCUSSION

Crystal Structures. Crystal structures of Ba_2MFeS_5 (M = Sb, Bi) were determined by use of single-crystal XRD, and the results suggest that the two isostructural compounds crystallize in the structural type of a Ba_3FeS_5 high-pressure phase with the orthorhombic space group *Pnma*.[3] In the following section, we will give detailed descriptions and comparisons for their structures.

The crystal structure of Ba_2SbFeS_5 is shown in Figure 1. There are two unique crystallographic Ba atoms, one M (M = Sb, Bi) atom, one Fe atom, and five S atoms in the asymmetric unit. All of the atoms are fully sited on the Wyckoff positions with no disordered atom occupancy. From Figure 1a, two-dimensional Sb−Fe−S layers stack along the a axis with Ba^{2+} cations inserted between the layers. While we examine one Sb−Fe−S layer in the bc plane separately, as shown in Figure 1b, it is found that the basic structural unit of compound Ba_2SbFeS_5 is an infinite 1-D ${}_1^{\infty}[SbFeS_5]^{4-}$ chain. The ${}_1^{\infty}[SbFeS_5]^{4-}$ chain is composed of vertex-converted SbS_5 tetragonal pyramids through edge sharing along b axis with FeS_4 tetrahedra alternately connected on both sides of a SbS_5 polyhedral chain. Similar 1-D chain structures were also reported in the chalcogenides of $FePb_4Sb_6S_{14}$ and $Fe_xPb_{4-x}Sb_4S_{10}$ ($0 \le x \le 2$).[22] Nevertheless, their 1-D chains are both formed from FeS_6 or $FeSe_6$ octahedra through direct edge sharing, while in the title compounds, the FeS_4 tetrahedra are bridged through intermediate MS polyhedra.

The coordination environments of Sb^{3+} ions can be described as asymmetric tetragonal pyramids with three short bond lengths (2.438−2.525 Å) and two longer ones (3.146 Å) for Sb−S bonds, which may be induced by the stereochemically active lone pair on Sb^{3+} ions (Figure 2a). However, when the farther neighboring S(3) atom with a bond length of 3.235 Å is considered, a distorted octahedron of SbS_6 indicates completeness. The Sb atom is seriously off from the center of the SbS_6 octahedron as a result of the electron-repulsion effect from the lone pair on Sb^{3+} ions with the bonding electron pairs on neighboring $S^{2-}(3)$ anions. Fe^{3+} features a tetrahedron coordination geometry with evident distortions compared with a

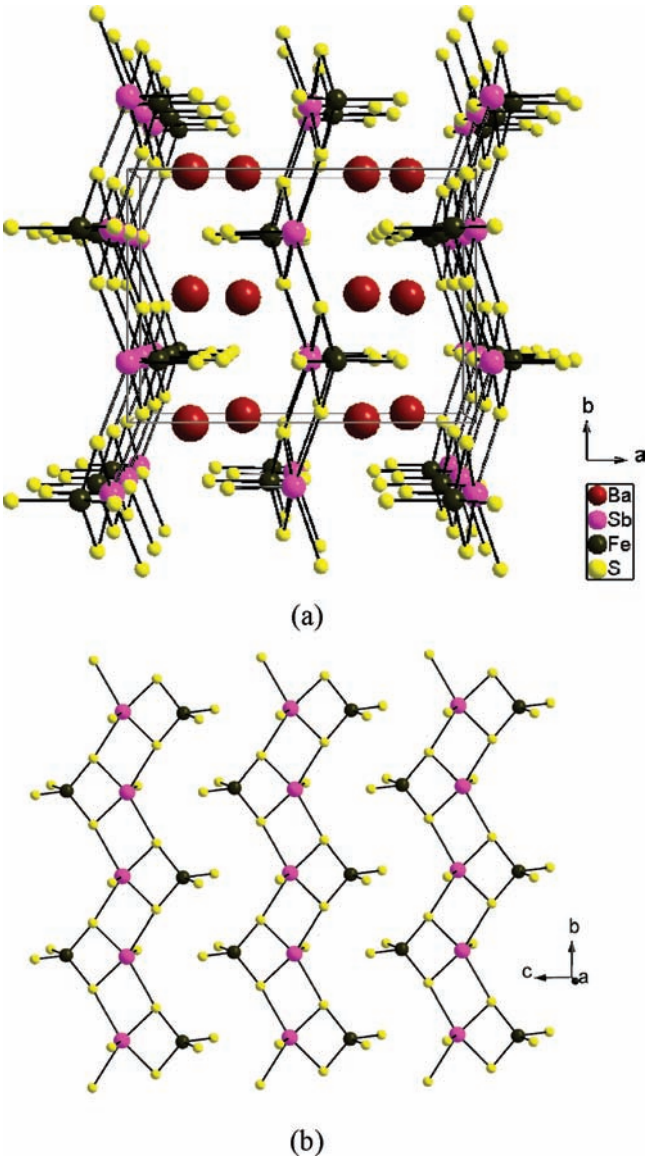

Figure 1. (a) Crystal structure of Ba_2SbFeS_5 viewed down the *c*-axis direction. (b) Structural unit of an infinite $_1^{\infty}[SbFeS_5]^{4-}$ chain arranged in the *bc* plane.

regular tetrahedron. The Fe−S bond lengths range from 2.209 to 2.229 Å and the S−Fe−S angles from 102.27 to 111.70° (Figure 2b).

Bond valence sum calculations performed on the Ba^{2+}, Sb^{3+}, and Fe^{3+} cations give reasonable values of 1.915, 3.298, and 3.000, respectively, which are well consistent with their normal valences (Table 3). The bond valence parameters summarized by Brese and O'Keeffe and by Brown were utilized in the calculations.[23] Owing to the existence of a steroactive lone pair on Sb^{3+} cations, most of the bond valence values are distributed over the three nearest S atoms, and less contribution is from the three farther S atoms. For Fe^{3+} cations, its oxidation state is also confirmed by the spin value fitted with the Curie−Weiss law from the $M-T$ magnetic measurements (see the next section).

The compounds Ba_2MFeS_5 (M = Sb, Bi) crystallize in the same structural type as that of a Ba_3FeS_5 high-pressure phase, in which one Ba is replaced by one Sb or Bi.[3] Hence, it is meaningful

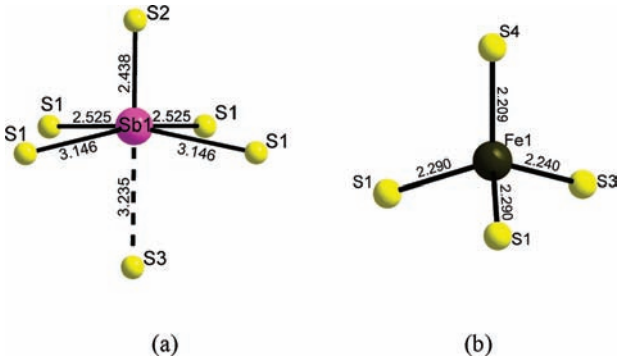

Figure 2. (a) Octahedral coordination environments of Sb^{3+} with ligand S atoms and (b) coordination geometry of a distorted FeS_4 tetrahedron.

to compare the crystal structures of the title compounds with their parent phase Ba_3FeS_5 in detail. For Ba_3FeS_5, there are two Wyckoff positions for Ba with Ba(1) on a general position (8d) and Ba(2) on a symmetry plane (4c) and one Wyckoff position for Fe(1) on a symmetry plane (4c), so the ratio of Ba/Fe is 3:1. While for the Ba_2MFeS_5 compounds there is only one Wyckoff position for Ba, i.e., Ba(1) on a general position (8d), Ba(2) on a symmetry plane in the case of Ba_3FeS_5 is now entirely substituted by M in Ba_2MFeS_5. Therefore, the total atom number of Ba in Ba_2MFeS_5 is twice that of M because Ba(1) occupies a general position, while M is located on a symmetry plane (see Table 2). As for Fe, they both lie on a (4c) position for Ba_3FeS_5 and Ba_2MFeS_5, respectively. The shortest distance of Fe−Fe is 6.273 Å in Ba_3FeS_5, while in Ba_2MFeS_5 compounds, their shortest distances are pulled closer because of the bridging Sb/Bi with values of 5.842 Å in Ba_2SbFeS_5 and 5.865 Å in Ba_2BiFeS_5. Figure 3 shows the structural relationship of Ba_3FeS_5 and Ba_2SbFeS_5 in terms of articulation of Ba(1)−S polyhedra. In both structures, six adjacent BaS polyhedral columns formed by face sharing along the *b* axis are further fused into distorted hexagonal rings through edge sharing. In fact, the main differences of the two structures are due to filling of the hexagonal rings. The isolated FeS_4 tetrahedra are separated by Ba(2) in Ba_3FeS_5, while in Ba_2MFeS_5, they are assembled into an infinite 1-D $_1^{\infty}[MFeS_5]^{4-}$ chain through intermediate M−S polyhedra. Thus, the paramagnetic property of Ba_3FeS_5 may result from the environmental locality of Fe^{4+} due to longer distances, and the antiferromagnetic property of Ba_2MFeS_5 may arise from electron-exchange interaction between the iron ions of inter- or intrachains through intermediate M−S polyhedra. We believe that substitution of one Ba by a Sb/Bi and a change of the oxidation state of Fe in Ba_3FeS_5 are responsible for the appearance of Fe−Fe antiferromagnetic coupling interactions in the Ba_2MFeS_5 compounds. It is a very interesting example for structure−magnetism relations.

Optical and Magnetic Properties. The UV−vis−NIR optical absorption spectra converted from the Kubelka−Munk equation for compounds Ba_2MFeS_5 (M = Sb, Bi) are plotted in Figure 4. The optical band gaps derived from the absorption spectra are ~0.95 eV for Ba_2SbFeS_5 and ~1.28 eV for Ba_2BiFeS_5, which are consistent with their black color.

The dc magnetic properties of compounds Ba_2MFeS_5 (M = Sb, Bi) were measured in the temperature range of 2−300 K at a magnetic field of 5000 Oe. The plots of $\chi - T$ and $1/\chi - T$ for polycrystalline Ba_2SbFeS_5 and Ba_2BiFeS_5 in the temperature

dx.doi.org/10.1021/ic102597y |*Inorg. Chem.* 2011, 50, 2378–2384

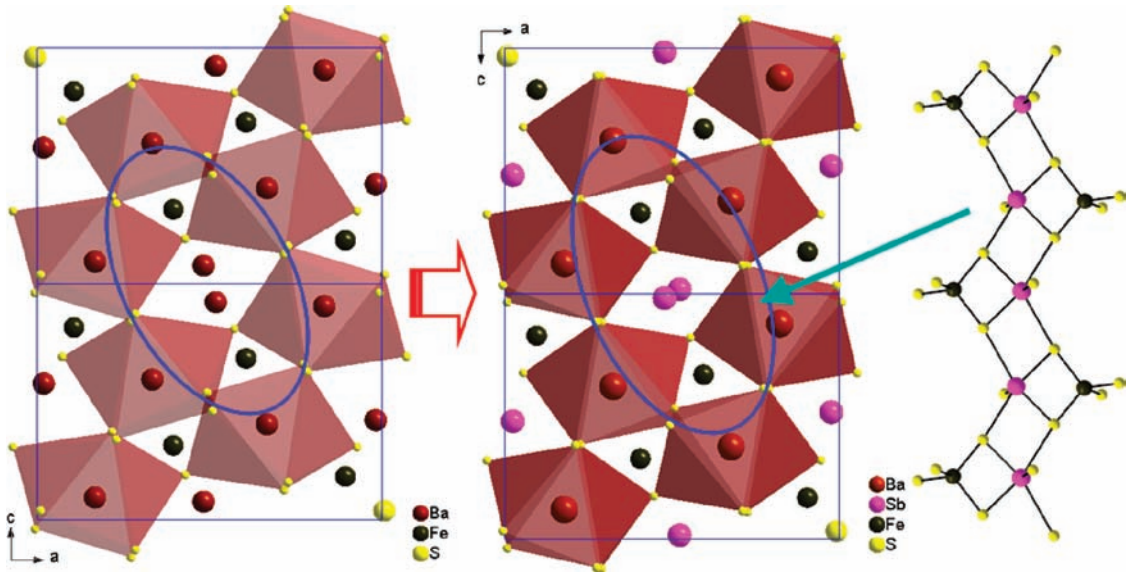

Figure 3. View of the two unit cells of Ba_3FeS_5 (left) and Ba_2SbFeS_5 (right) along the [010] direction. The Ba(1) atoms are represented as Ba−S polyhedra above both structures. The inset is the $_1^{\infty}[SbFeS_5]^{4-}$ chain in Ba_2SbFeS_5.

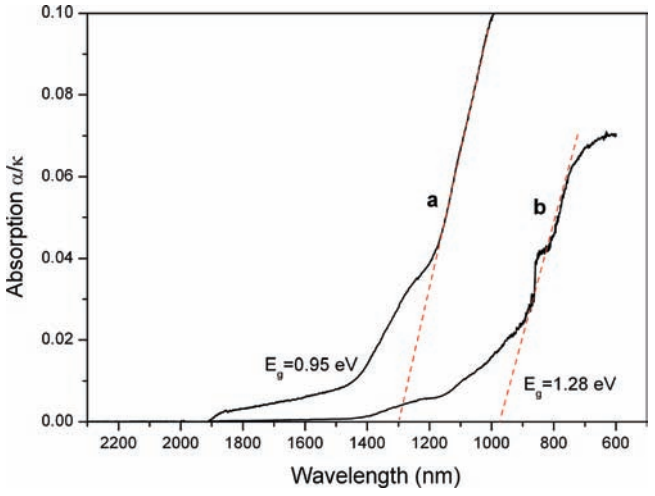

Figure 4. Optical absorption spectra converted from diffuse-reflectance spectra using the Kubelka−Munk equation for powder samples of (a) Ba_2SbFeS_5 and (b) Ba_2BiFeS_5.

range of 2−300 K are shown in Figure 5a,b. The magnetic susceptibility shows a maximum peak at 13 and 35 K for Ba_2SbFeS_5 and Ba_2BiFeS_5, respectively, indicating the presence of antiferromagnetic interactions below their Néel temperature. Above the Néel temperature, the susceptibility increases with a decrease in the temperature, exhibiting typical Curie−Weiss behavior. The Curie−Weiss equation fitting of the susceptibility data above the antiferromagnetic transition temperature yields values of the Curie constant $C = 3.24(2)$ emu K mol^{-1} and the Weiss constant $\theta = -67.65(2)$ K for Ba_2SbFeS_5 and $C = 4.01(1)$ emu K mol^{-1} and $\theta = -64.67(3)$ K for Ba_2BiFeS_5. The effective magnetic moments of Fe^{3+} ions in Ba_2SbFeS_5 and Ba_2BiFeS_5 are calculated to be 5.09(1) and 5.66(3) μ_B, respectively, which are close to the value of 5.91(6) μ_B obtained by the high-spin Fe^{3+} ($S = {}^5/_2$) ion, indicating that Fe^{3+} ions have a high-spin state and a small orbital moment contribution in the tetrahedral FeS_4 configuration. For compound Ba_2BiFeS_5, magnetization (M) as a function of the applied magnetic field (H) was done at $T = 2$ K, and a linear increase in the magnetization was observed, which are in agreement with an antiferromagnetic ordering below 35 K (Figure S3 in the Supporting Information).[24] So, the uptilt of the magnetic susceptibility for Ba_2BiFeS_5 in a low-temperature zone may arise from the other impurities.

Band Structures and DOSs. The band-structure calculations were performed for the title compounds with α (up) and β (down) spin configurations of Fe^{3+} ions because they exhibit antiferromagnetic ordering below the transition temperature. The band structure of Ba_2SbFeS_5 along high symmetry points of the first Brillouin zone (BZ) is plotted in Figure 6a as a representative of the Ba_2MFeS_5 (M = Sb, Bi) compounds because of their similar band structures. The special k points in the first BZ are defined in Table S1 in the Supporting Information. The conduction band minimum is located at the Z point of the BZ, while the valence band maximum is located near the X point along the XΓ line with an energy difference of 0.99 eV, indicating that the compound belongs to an indirect-band semiconductor. The calculated band gap is in good agreement with the one estimated from the optical experiments.

From the band structure and total and partial DOSs of Ba_2SbFeS_5 as shown in Figure 6a,b, except for the innermost localized Ba 5s orbital, there are three sections from −14 eV to the VBM, i.e., the Fermi level. The first section from −14 to −10 eV is mainly composed of the inner Ba 5p and S 3s orbitals as well as a few Sb 5s5p states. The next section, located around −7 eV, is mostly contributed by Fe 3d and Sb 5s states with some mixing of S 3p states. This segment exhibits a sharp and narrow shape owing to the localizability of the Fe 3d orbitals. The third band region extending from −5 eV to the Fermi level, which constitutes the valence band, is mainly composed of Sb 5p and S 3p states with small mixtures of Fe 3d4p states. The S 3p states are the main components in the valence band, especially around the Fermi level. Above the Fermi level around 1 eV, it is a narrow-shaped conduction band composed of S 3p and Fe 3d states with small mixings of Fe 4p and Sb 5p states, while from 2 to 4 eV, it is another expanded band composed of S 3p, Fe 3d, and Sb 5p

dx.doi.org/10.1021/ic102597y |*Inorg. Chem.* 2011, 50, 2378–2384

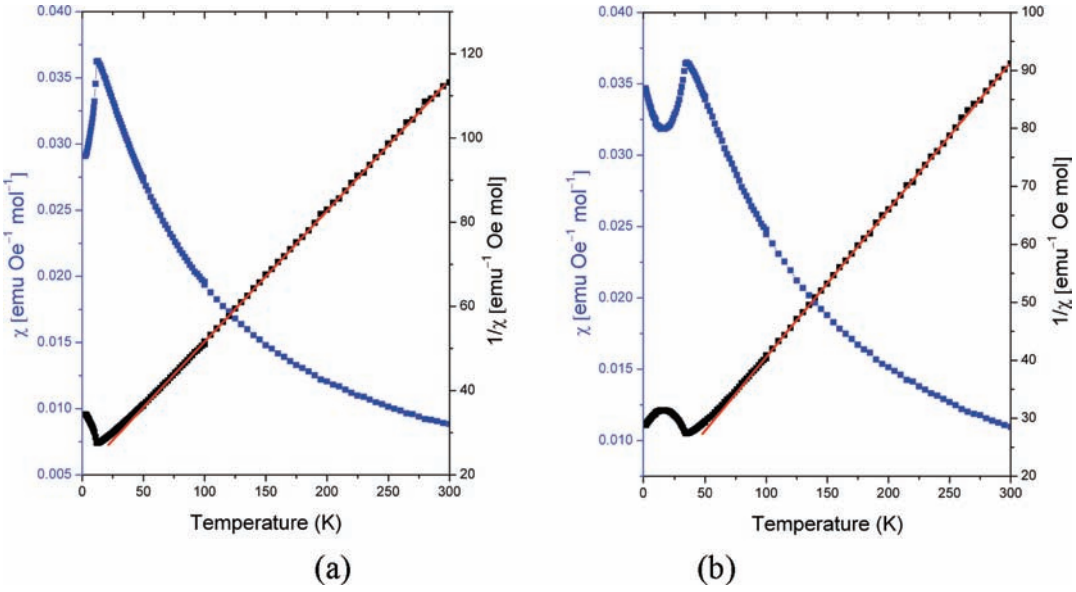

Figure 5. Plots of $1/\chi$ vs T and χ vs T for polycrystalline (a) Ba_2SbFeS_5 and (b) Ba_2BiFeS_5 in the temperature range of 2−300 K. The red lines represent the linear fits of the data above the Néel temperature T_N according to the Curie−Weiss law.

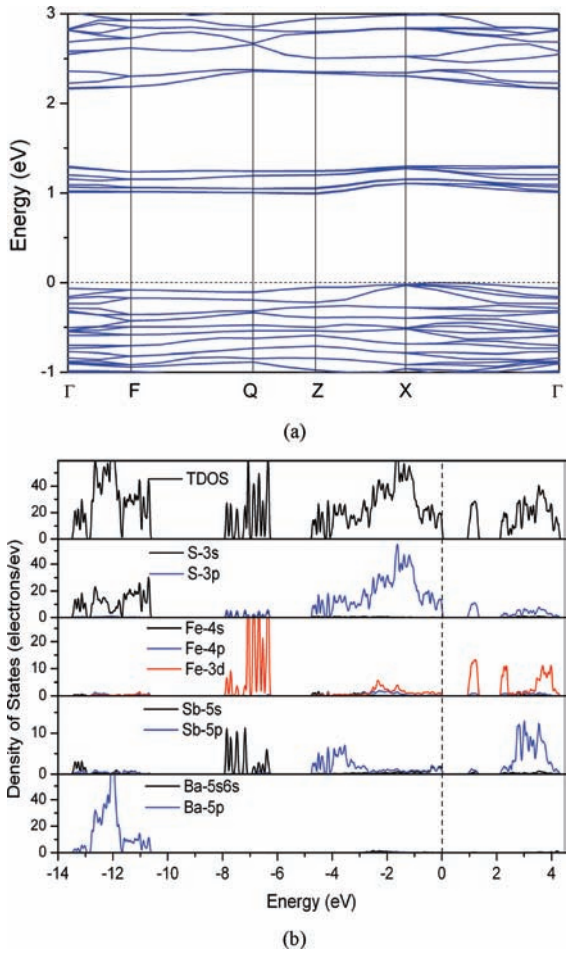

Figure 6. (a) Electronic energy band structures and (b) total and partial DOSs for Ba_2SbFeS_5. The Fermi level is set at 0 eV.

states. From the partial DOSs, we can see that there are strong orbital hybridizations between Fe 3d and S 3p orbitals around 1 eV in the conduction band. Accordingly, the optical absorption peaks close to the near-IR edge can be mainly assigned as charge transfers from the occupied S 3p states to the unoccupied Fe 3d states for compounds Ba_2BiFeS_5 and Ba_2SbFeS_5, respectively.

CONCLUSIONS

We have synthesized and structurally characterized two new quaternary antiferromagnetic sulfides, Ba_2SbFeS_5 and Ba_2BiFeS_5. Magnetic measurements indicated that the two compounds are both antiferromagnetic materials with Néel temperatures of 13 and 35 K for Ba_2SbFeS_5 and Ba_2BiFeS_5, respectively. The Curie−Weiss equation fitting of the susceptibility data above the transition temperature shows that Fe^{3+} ions have a high-spin state and a small orbital moment contribution in the tetrahedral FeS_4 configuration. The two compounds are isostructural and crystallize in the structural type of a Ba_3FeS_5 high-pressure phase. As an interesting result, substitution of one Ba^{2+} by a Sb^{3+}/Bi^{3+} and an oxidation state change of iron from Fe^{4+} to Fe^{3+} give rise to the occurrence of Fe−Fe antiferromagnetic coupling interactions in the Ba_2MFeS_5 compounds. The UV−vis−NIR optical absorption spectra converted from the Kubelka−Munk equation give optical band gaps of 0.95 eV for Ba_2SbFeS_5 and 1.28 eV for Ba_2BiFeS_5, which are assigned to charge transfers from the occupied S 3p states to the unoccupied Fe 3d states in view of the first-principles DFT computations of band structures and DOSs.

ASSOCIATED CONTENT

Supporting Information. X-ray crystallographic files in CIF format, simulated and experimental powder XRD patterns for Ba_2SbFeS_5 and Ba_2BiFeS_5, definitions of the special k points in the first BZ, and plots of M (magnetization) vs H (magnetic field) for polycrystalline Ba_2BiFeS_5 at T = 2 K. This material is available free of charge via the Internet at http://pubs.acs.org.

dx.doi.org/10.1021/ic102597y |*Inorg. Chem.* 2011, 50, 2378–2384

AUTHOR INFORMATION

Corresponding Author
*E-mail: cwd@fjirsm.ac.cn.

ACKNOWLEDGMENT

This investigation was based on work supported by the National Natural Science Foundation of China under Project 20773131, the National Basic Research Program of China (No. 2007CB815307), the Funds of Chinese Academy of Sciences (KJCX2-YW-H01), and Fujian Key Laboratory of Nanomaterials (No. 2006L2005).

REFERENCES

(1) Grey, I. E.; Hong, H.; Steinfink, H. *Inorg. Chem.* **1971**, *10*, 340–343.
(2) Hong, H. Y.; Steinfink, H. *J. Solid State Chem.* **1972**, *5*, 93–104.
(3) Lemley, J. T.; Jenks, J. M.; Hoggins, J. T.; Eliezer, Z.; Steinfink, H. *J. Solid State Chem.* **1976**, *16*, 117–128.
(4) Hoggins, J. T.; Rendondiazmiron, L. E.; Steinfink, H. *J. Solid State Chem.* **1977**, *21*, 79–90.
(5) Cohen, S.; Rendondiazmiron, L. E.; Steinfink, H. *J. Solid State Chem.* **1978**, *25*, 179–187.
(6) Jenks, J. M.; Hoggins, J. T.; Rendondiazmiron, L. E.; Cohen, S.; Steinfink, H. *Inorg. Chem.* **1978**, *17*, 1773–1775.
(7) Swinnea, J. S.; Steinfink, H. *J. Solid State Chem.* **1980**, *32*, 329–334.
(8) Swinnea, J. S.; Eisman, G. A.; Perng, T. P.; Kimizuka, N.; Steinfink, H. *J. Solid State Chem.* **1982**, *41*, 104–108.
(9) Ino, K.; Wakeshima, M.; Hinatsu, Y. *Mater. Res. Bull.* **2001**, *36*, 2207–2213.
(10) Dorrscheidt, W.; Schafer, H. *Z. Naturforsch., B: J. Chem. Sci.* **1981**, *36*, 410–414.
(11) Cordier, G.; Schwidetzky, C.; Schafer, H. *J. Solid State Chem.* **1984**, *54*, 84–88.
(12) Aurivillius, B. *Acta Chem. Scand. A* **1983**, *37*, 399−407.
(13) Choi, K.-S.; Kanatzidis, M. G. *Inorg. Chem.* **2000**, *39*, 5655–5662.
(14) Choi, K. S.; Iordanidis, L.; Chondroudis, K.; Kanatzidis, M. G. *Inorg. Chem.* **1997**, *36*, 3804–3805.
(15) (a) Egorova, B. V.; Olenev, A. V.; Berdonosov, P. S.; Kuznetsov, A. N.; Stefanovich, S. Y.; Dolgikh, V. A.; Mahenthirarajah, T.; Lightfoot, P. *J. Solid State Chem.* **2008**, *181*, 1891–1898. (b) Zhang, W. L.; Lin, X. S.; Zhang, H.; Wang, J. Y.; Lin, C. S.; He, Z. Z.; Cheng, W. D. *Dalton. Trans.* **2010**, *39*, 1546–1551. (c) Gave, M. A.; Malliakas, C. D.; Weliky, D. P.; Kanatzidis, M. G. *Inorg. Chem.* **2007**, *46*, 3632–3644. (d) Iordanidis, L.; Bilc, D.; Mahanti, S. D.; Kanatzidis, M. G. *J. Am. Chem. Soc.* **2003**, *125*, 13741–13752.
(16) Sheldrick, G. M. *SHELXTL-97*; University of Göttingen: Göttingen, Germany, 1997.
(17) O'Connor, C. J. *Prog. Inorg. Chem.* **1982**, *29*, 203–283.
(18) Clark, S. J.; Segall, M. D.; Pickard, C. J.; Hasnip, P. J.; Probert, M. J.; Refson, K.; Payne, M. C. *Z. Kristallogr.* **2005**, *220*, 567–570.
(19) Perdew, J. P.; Burke, K.; Ernzerhof, M. *Phys. Rev. Lett.* **1996**, *77*, 3865–3868.
(20) Payne, M. C.; Teter, M. P.; Allan, D. C.; Arias, T. A.; Joannopoulos, J. D. *Rev. Mod. Phys.* **1992**, *64*, 1045–1097.
(21) (a) Cococcioni, M.; de Gironcoli, S. *Phys. Rev. B* **2005**, *71*, 035105. (b) Dudarev, S. L.; Botton, G. A.; Savrasov, S. Y.; Humphreys, C. J.; Sutton, A. P. *Phys. Rev. B* **1998**, *57*, 1505–1509.
(22) (a) Derakhshan, S.; Assoud, A.; Soheilnia, N.; Kleinke, H. *J. Alloys Compd.* **2005**, *390*, 51–54. (b) Matsushita, Y.; Ueda, Y. *Inorg. Chem.* **2003**, *42*, 7830–7838. (c) Poudeu, P. F. P.; Takas, N.; Anglin, C.; Eastwood, J.; Rivera, A. *J. Am. Chem. Soc.* **2010**, *132*, 5751–5760.
(23) (a) Brese, N. E.; O'Keeffe, M. *Acta Crystallogr., Sect. B* **1991**, *47*, 192–197.(b) Brown, I. D. *The Chemical Bond in Inorganic Chemistry: The Bond Valence Model*; Oxford University Press: New York, 2002.
(24) Zhang, W. L.; Cheng, W. D.; Zhang, H.; Geng, L.; Li, Y. Y.; Lin, C. S.; He, Z. Z. *Inorg. Chem.* **2010**, *49*, 2550–2556.